# High-$T_C$ superconducting THz emitters fabricated by wet etching

Yuuki Shibano, Takanari Kashiwagi, Yuki Komori, Kazuki Sakamoto, Yuki Tanabe, Takashi Yamamoto, Hidetoshi Minami, Richard A. Klemm [iD], and Kazuo Kadowaki [iD]

## ARTICLES YOU MAY BE INTERESTED IN

Improved excitation mode selectivity of high-$T_c$ superconducting terahertz emitters
Journal of Applied Physics **124**, 033901 (2018); https://doi.org/10.1063/1.5033914

Circularly polarized terahertz radiation monolithically generated by cylindrical mesas of intrinsic Josephson junctions
Applied Physics Letters **113**, 052601 (2018); https://doi.org/10.1063/1.5040159

Thermoreflectance microscopy measurements of the Joule heating characteristics of high-$T_c$ superconducting terahertz emitters
Journal of Applied Physics **122**, 233902 (2017); https://doi.org/10.1063/1.5002743

# High-$T_c$ superconducting THz emitters fabricated by wet etching

View Online    Export Citation    CrossMark

Yuuki Shibano,[1] Takanari Kashiwagi,[1,2,a] Yuki Komori,[1] Kazuki Sakamoto,[1] Yuki Tanabe,[1] Takashi Yamamoto,[3] Hidetoshi Minami,[1,2] Richard A. Klemm,[4] and Kazuo Kadowaki[1,2,5]

## AFFILIATIONS

[1] Graduate School of Pure & Applied Sciences, University of Tsukuba, 1-1-1 Tennodai, Tsukuba, Ibaraki 305-8573, Japan

[2] Division of Materials Science, Faculty of Pure & Applied Sciences, University of Tsukuba, 1-1-1, Tennodai, Tsukuba, Ibaraki 305-8573, Japan

[3] QuTech, Delft University of Technology, PO Box 5046, 2600 GA Delft, The Netherlands

[4] Department of Physics, University of Central Florida, 4111 Libra Drive, Orlando, Florida 32816-2385, USA

[5] Algae-Biomass and Energy System(ABES) Research & Development Center, University of Tsukuba, 1-1-1 Tennodai, Tsukuba, Ibaraki 305-8572, Japan

[a] kashiwagi@ims.tsukuba.ac.jp

## ABSTRACT

We studied the etching of small crystals of the high-$T_c$ superconductor $Bi_2Sr_2CaCu_2O_{8+\delta}$ (Bi2212) with various dilute compositions of hydrochloric and nitric acids. A particular mixture of those acids was chosen to simultaneously fabricate multiple rectangular stand-alone Bi2212 mesa structures from a large, doubly-cleaved and doubly metallic-coated single crystal. The radiation characteristics of these devices were found to be very similar to stand-alone devices fabricated previously using dry-etching techniques. The greatly reduced time and cost of fabrication of stand-alone Bi2212 devices using our wet-etching technique should facilitate the mass production of a large number of identical stand-alone devices from a large single-crystalline Bi2212 substrate.

## I. INTRODUCTION

In a single crystal of the high-$T_c$ superconductor $Bi_2Sr_2CaCu_2O_{8+\delta}$ (Bi2212), the superconducting $CuO_2$ layers sandwiched by the insulating $Bi_2O_2$ layers are stacked along the crystallographic $c$-axis. This stacking structure is well known to form a one-dimensional stack of identical intrinsic Josephson junctions (IJJs).[1–3] Because of this natural IJJ stacking in Bi2212 single crystals, a small Bi2212 mesa structure acts as a THz emitter when a dc voltage is applied across the junctions.[4] The dc voltage applied across the stack of IJJs drives an ac current to generate THz emission from the IJJs according to the ac Josephson effect.[5] The mesa structure also behaves as an electromagnetic (EM) cavity, with standing wave modes depending upon its geometrical shape. When the frequency of the ac current in IJJs matches the resonance frequency of a cavity mode, strongly enhanced EM waves in THz region are produced.[4,6–8]

According to previous studies, radiation frequencies ranging from 0.3 to 2.4 THz were observed from Bi2212-THz emitters.[9–12] The maximum output power was found to be about 30 ~100 $\mu$W from a single mesa device.[9,12–15] By synchronizing three mesa structures, a 0.6 mW level of output power was reported.[15] Very recently, from thinner and narrower rectangular Bi2212 devices, emissions ranging from 1 ~11 THz were reported.[16]

Due to recent technical progress in semiconducting devices such as quantum cascade lasers and resonant tunneling diodes,[17,18] their THz-emitting properties are comparable with the characteristic features of the Bi2212-THz emitters mentioned above, since both types of devices have

the potential to operate as compact solid state oscillators in THz region.[19] But none of the semiconducting devices can yet span the overall 0.3-11 THz range of the Bi2212-THz emitters.[11,12,16] Details of the development of the Bi2212-THz emitters were reviewed recently.[20–22]

In order to further develop the device characteristics and to lower the costs of production of Bi2212-THz emitters, improvements in the fabrication techniques and processes of the mesa devices are required. Most mesa structures of Bi2212 single crystals studied previously were fabricated using dry-etching techniques such as ion milling with a metallic mask[6] or focused ion beam milling.[8] However, several groups recently reported wet-etching fabrication methods of mesa structures from Bi2212 single crystals.[23–25]

Based upon those studies,[23–25] we extended their wet-etching methods to fabricate stand-alone mesa (SAM) structures. A SAM not only does not have a superconducting substrate underneath it, its top and bottom surfaces are coated with gold, providing more efficient self-generated heat exhaust from the mesa devices, and hence increasing the device's output radiation power and frequency range. These characteristics were predicted theoretically[26,27] and have been confirmed experimentally.[9–12]

In this report, we first discuss the etching of Bi2212 single-crystal using various concentrations of three different types of wet etchants. Then, details of the wet-etching SAM fabrication process and the characteristics of the fabricated SAMs are briefly described. The wet-etched SAM device characteristics are then shown to be consistent with those obtained from SAMs fabricated using the more expensive and time-consuming dry-etching methods.

## II. WET-ETCHING STUDIES OF Bi2212 SINGLE CRYSTALS

In previous studies,[23–25] wet etching of a single crystal of Bi2212 with dilute hydrochloric acid was shown to transform the etched region into insulating BiOCl. When a very dilute HCl solution with pH = 1.65 was used, the transformation of Bi2212 to BiOCl was only observed on the surface of Bi2212 single crystals.[23] However, when a higher concentration of HCl was used, the etched depth of 7 $\mu$m could be achieved.[25] Those authors used the 1:8 HCl to water solution,[25] which is 30~50 times more concentrated than that of the dilute HCl solutions used in the earlier studies of Kato et al. and Nishikawa et al.[23,24]

In expanding upon those three studies, we studied the etching effects of several dilute water solutions of concentrated (11.7 M) HCl, concentrated (13.0 M) HNO$_3$, and mixed aqueous solutions of those acids. The amounts in mL of those acids added to 25 mL of water to prepare each of the tested solutions are summarized in Table I.

In order to investigate the etching characteristics of the solutions detailed in Table I under conditions suitable for SAM production, we first prepared test samples of a single

**TABLE I**. List of tested solutions.

| Solution name | 11.7 M HCl | 13.0 M HNO$_3$ | H$_2$O |
|---|---|---|---|
| A-1 | - | 1.0 mL | 25 mL |
| A-2 | - | 2.0 mL | 25 mL |
| A-3 | - | 3.0 mL | 25 mL |
| B-1 | 0.3 mL | - | 25 mL |
| B-2 | 1.0 mL | - | 25 mL |
| B-3 | 3.0 mL | - | 25 mL |
| C-1 | 0.3 mL | 2.0 mL | 25 mL |
| C-2 | 0.5 mL | 2.0 mL | 25 mL |
| C-3 | 1.0 mL | 2.0 mL | 25 mL |

crystal of Bi2212 whose top surface was patterned by photoresist (TOKYO OHKA KOGYO CO., OFPR-800) using a micro-pattern generator (Heidelberg Instruments, $\mu$PG501). Each test sample was placed in an etchant solution for several seconds. Then, it was washed with water while under exposure to ultrasonic vibrations. Finally, the height difference between the top and bottom of the photoresist pattern, corresponding to the reduction in the height (or the increase in the depth of the etching pattern) of the mesa structure, was measured by atomic force microscopy (AFM) (KEYENCE Co., VN-8000). These processes were repeated several times in order to check the progress of the etching process. An optical photograph and a schematic sketch of the procedure used to check the etching progress are displayed in Fig. 1.

We first describe the results of the dilute HNO$_3$ etchant solutions named A-1, A-2 and A-3 in Table I. In these cases, the obtained reduction in the height of the mesa structure is proportional to the etching time. The etching rates along the crystallographic c-axis were estimated to be about 10~20 nm/s. These rates were estimated from the total etching time of 50 s. The etching rate along the c-axis was nearly the same for all three HNO$_3$ concentrations studied. However, the etching rate along the ab-plane increases with increasing HNO$_3$ concentration. Unfortunately, etching along the ab-plane allows for the occurrence of an "undercut", in which the etching extends underneath the photoresist pattern. Since the undercutting can occur in irregular shapes, a large photoresist undercut prevented us from producing the desired shape and size of the mesa structure. In addition, it often created an electrical leakage of the electrodes between the top and bottom of the mesa structure, rendering the sample useless for THz emission control. Further details of the etching rate along the ab-plane in each of the steps have not yet been obtained, because the etching distance along the ab-plane could not be determined precisely without removing the photoresist pattern placed on the top surface of the Bi2212 single crystal.

However, the total size of the undercut after etching can be estimated very roughly from optical photographs of the samples. If there are large undercuts of the sample, the optical photographs of the samples show clear changes in the colors and/or shapes around the edges of the photoresist patterns.
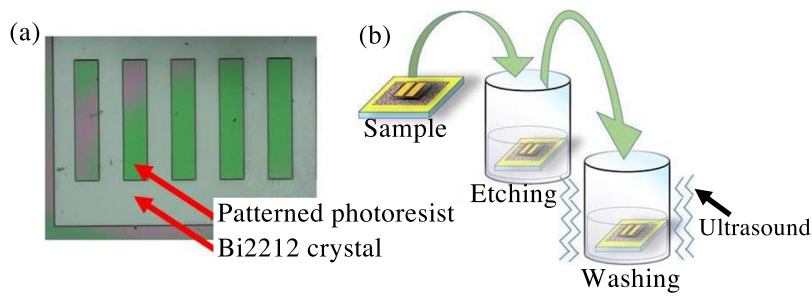
**FIG. 1**. (a) Optical photograph of a test sample used to check the quality of the etching. A rectangular shape of photoresist was patterned on the cleaved surface of a piece of a Bi2212 single crystal. (b) Schematic picture of the procedure for checking the etching progress. First, a sample was prepared by patterning photoresist on a cleaved Bi2212 crystal surface. Then, the sample was placed in the etching solution for several seconds. After that the sample was dipped and washed and shaken in an ultrasonic water bath. Then, the height difference between top and bottom of the photoresist pattern was measured by the AFM. These processes were repeated several times.

This color changes indicate roughly the sizes of the undercuts. From this point of view, the approximate sizes of the undercuts are on the order of 5~10 $\mu$m and ~15 $\mu$m, which are observed respectively for solutions A-2 and A-3 after the etching time of 40 s.

Next, we describe the results of etching Bi2212 with the dilute HCl solutions B-1, B-2 and B-3 listed in Table I. For the B-1 solution, the etching along the crystallographic *c*-axis progresses only up to 0.2 $\mu$m thickness and no undercut of the photoresist was observed after a total etching time of 50 s. This "soft" etching characteristic is very desirable for sample preparation, and is consistent with a previous study.[23] According to that study,[23] it was also known that the etched part of the Bi2212 single crystal was transformed to BiOCl by using a dilute HCl solution as the etchant. One possible reason of this soft etching characteristic may be due to the reacted BiOCl covering the top surface of the Bi2212 crystal, acting as a barrier to further etching.

On the other hand, the etching along the crystallographic *c*-axis and along the *ab*-plane both progressed with increasing the concentration of HCl. The solutions B-2 and B-3 gave rise to almost linear relations of the reduction in the mesa thickness with the increase in HCl concentration and with the etching rate. The etching rates were estimated to be on the order of 60 ~80 nm/s. These values were estimated from the total etching time of 50 s. This stronger etching characteristic with increasing HCl concentration is also consistent with a previous study using a more concentrated HCl solution in water.[25] The HCl concentration of B-3 is comparable to the previously studied 1:8 water solution of HCl.[25] In order to obtain reliable data on the etching rates, it is most important to remove the BiOCl that formed and accumulated on the surface of the Bi2212 crystal during the etching with HCl.

The results obtained from the HCl solutions B-1 to B-3 and from a previous study[25] clearly indicate that the mesa structure can be fabricated by an appropriate concentration of HCl solution. However, higher concentrations of HCl cause larger undercuts of the photoresist on the sample surface. Therefore, a particular HCl concentration should be selected in accordance with the desired size and thickness of the mesa structures to be fabricated. It is noted that the approximate

sizes of the undercuts on the order of ~5 $\mu$m and ~10 $\mu$m are observed respectively for solutions B-2 and B-3 after the etching time of 40 s. These sizes are estimated from the optical photographs of the samples as for the cases using the A solutions.

We also studied the etching effects of mixtures of the above two acid solutions. The concentration of HCl in solution C-1 is slightly lower than that of B-1. However, we can obtain more than a 4 $\mu$m reduction in the height of the mesa after a total etching time of 50 s. This result suggests that the BiOCl material formed on the surface of Bi2212 crystal can efficiently be simultaneously removed and washed by using that mixture of HCl and HNO$_3$ solutions.

With increasing the HCl concentration in solutions C-2 and C-3 as described in Table I, the etching rate only slightly increases over that of solution C-1. In addition to that, by using either the C-2 or C-3 solutions, the top surface of the Bi2212 crystal appears to be etched more uniformly than that etched with the C-1 solution. This etching characteristic can be seen in the optical photograph of each etching step, as shown in Fig. 2(b). This uniform etching characteristic is also important in fabricating the desired shapes of the mesa structures. The etching rates along the crystallographic *c*-axis for the three solutions C-1, C-2 and C-3 remain in the range 80 ~100 nm/s, which are higher than those obtained from the pure HCl solutions studied.

Moreover, the undercuts of the photoresist on the sample produced using the C solutions were less significant than was found using the pure HCl solutions B-2 and B-3. Those are on the order of a few $\mu$m after an etching time of 40 s, which are estimated from the optical photographs as mentioned above. As shown in Fig. 2(b), the changes in color and/or shape around the edges of the photoresist patterns are not clearly observable. This fact indicates that small undercuts can be obtained by using the C solutions. Therefore, this result suggests that the mixed HCl and HNO$_3$ solutions are better than any of the single-acid A or B solutions for selectively etching along the crystallographic *c*-axis of a Bi2212 single crystal. It is also noted that the effect of the undercuts of the solution C-1 may be the smallest of the three C solutions. The undercut size increases with increasing HCl concentration in the C solution.
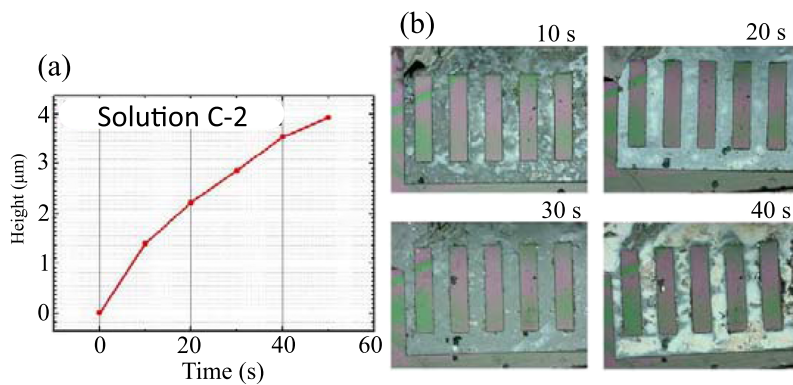
FIG. 2. (a) An example of the increase in the height of the etched portion of the mesa (or decrease in the overall height of the Bi2212 mesa) as a function of the etching time measured using solution C-2. (b) Optical photographs of the mesa taken after each 10 second interval during wet etching with solution C-2.

The etching characteristics observed using solution C-2 are shown in Fig. 2. The reduction in the height of the mesa structure increases with increasing the etching time as shown in Fig. 2(a). The etching progresses on the surface of the sample depending on the etching time are displayed in Fig. 2(b). It is noted that the etching rate shown in Fig. 2(a) is only an example, and it sometimes strongly depends on other features of the preparation conditions, such as the washing process, *etc.* However, by carefully controlling the preparation details, the pictured tendency of the etching rate was found to be quite reproducible.

According to the above results, the C-2 solution was found to be most suitable for fabricating final mesa structures a few micrometers in height with limited amounts of under-cutting of the photoresist. In the next section, the actual fabrication process of SAMs using this C-2 solution is described in detail.

## III. FABRICATION OF SAMS BY WET ETCHING

Prior to the etching process, we first doubly cleave a piece of a Bi2212 single crystal a few micrometers thick and several mm wide in both lateral directions with Scotch tape. Note that high-quality single crystals of Bi2212 were grown by the traveling solvent floating zone method using a modified infrared image furnace (Canon Machinery Inc.).[28] Both freshly cleaved surfaces of the thin crystal were first coated with Ag and then with Au by evaporation. The thicknesses of these evaporated metals are each about 10 nm. This thin doubly-metal-coated, doubly-cleaved sample is fixed onto a $7 \times 7 \times 0.5$ mm$^3$ sapphire substrate with silver paste. In order to harden the silver paste, the sample was baked by a hot plate at 140 °C for 10 min. Next, the top of the sample was coated with photoresist using a spin coater at 6,000 rpm for 20 s. It was then baked at 90 °C for 5 min. The photoresist on the sample top was exposed using the micro-pattern generator, and then it was patterned into



(1) Patterning of photoresist

(2) Ar ion milling
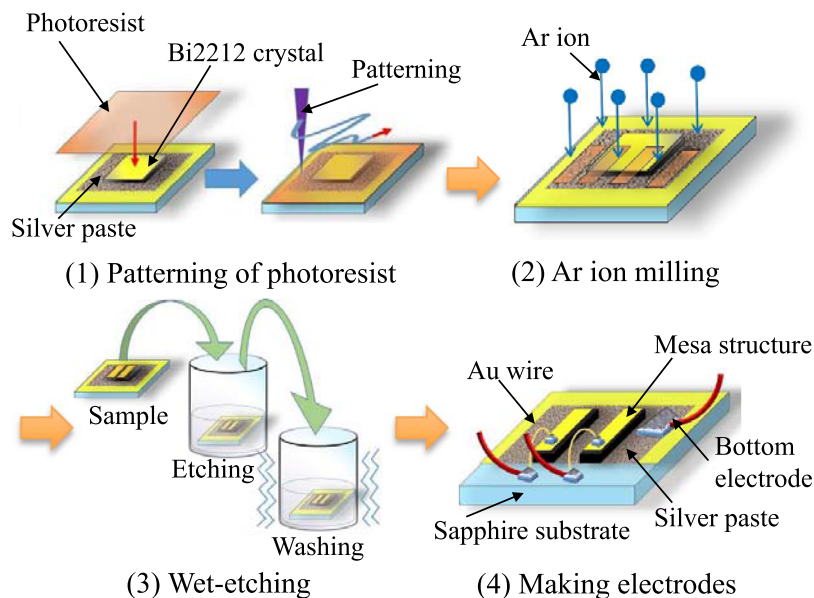
(3) Wet-etching

(4) Making electrodes

FIG. 3. Schematic sketches of the wet-etching SAM fabrication process. (1) Patterning of the photoresist with the micro-pattern generator. (2) Removing the metallic films except for the photoresist patterns. (3) Wet-etching process of the sample. (4) Attaching the electrical wirings.

seven rectangles, each of dimensions of 80×300 $\mu$m$^2$ by exposing it to a liquid solution (TOKYO OHKA KOGYO CO., NMD-3) and water, as shown in Fig. 3–(1). Then the sample was again baked at 90 °C for 5 min in order to stabilize the photoresist on the top of the thin crystal.

Next, we removed the metallic films in-between the rectangular photoresist patterns on the top of the single crystal of Bi2212 by Ar ion milling at a microwave power of 100 W and acceleration voltage of 300 V for 5 min, as pictured in Fig. 3–(2). Note that the subsequent etching of the sample progresses from the resulting exposed portions of the top surface of the Bi2212 single crystals which are not covered by the metallic films and the photoresist.

The sample as prepared above was first etched with solution C-2 as shown in Fig. 3–(3) for 5 s, and then washed in pure water while shaken with ultrasound for ~5 s. This etching and washing process was repeated several times, until the etching extended through the entire thickness of the exposed portions of the Bi2212 crystal. Then, the top photoresist regions were removed using acetone. Finally, the top and bottom electrodes were prepared by attaching Au and Cu wires with Ag paste as shown in Fig. 3–(4). From this procedure, the resulting SAM structures were constructed. It is noted that this repeated
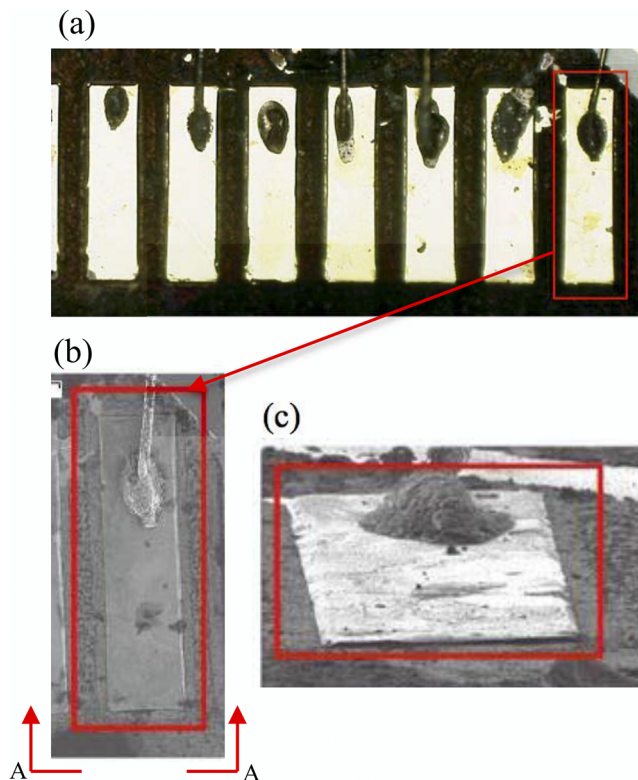


**FIG. 4**. (a) An optical photograph of the SAMs fabricated by wet etching. (b) An SIM image of the sample measured for its radiation characteristics. (c) An SIM image taken along the A-A direction in (b).

washing process may be helpful in removing deposited materials such as BiOCl quickly and more smoothly from the edges of the mesa structures and surfaces of Bi2212 crystals. In this experiment, we used this repeated washing process based upon the result of Section II. The details of the effectiveness of this repeated washing process will be reported in future works.

Figure 4(a) shows an optical photograph of the seven SAMs fabricated simultaneously with the described wet-etching method using solution C-2. Scanning ion microscope (SIM) images of the SAM are shown in Fig. 4(b) and 4(c). The dimensions of the mesa structures are 71-83 × 291-303 × 2.5 $\mu$m$^3$. The width, length, and thickness of the mesa structures were estimated using AFM and an optical microscope. The length and width of the mesa structure are estimated by considering the overall undercut effect. The above thickness of the mesa structure includes the thickness of the evaporated metals.

The top electrical contact was made from a gold wire with a diameter of 10 $\mu$m. This gold wire was fixed on the top surface of the SAM by using silver paste as shown in Fig. 4. Since the SAM was originally fixed onto the sapphire substrate by silver paste, the silver paste itself comprises the bottom electrode of each SAM, as displayed in Fig. 3–(4). In the next section, we describe the radiation characteristics of one of these SAMs.

## IV. RADIATION CHARACTERISTICS OF A SAM FABRICATED BY WET ETCHING

We fabricated seven SAMs using the above wet-etching technique and measured the EM waves from these SAMs. Here, we show the radiation characteristics of one of them shown in Fig. 4. The temperature dependence of the $c$-axis resistance of that SAM is shown in Fig. 5(a). The resistance increases with decreasing the mesa temperature and the superconducting transition is observed around 78 K. Below that transition, a contact resistance of 5~6 Ω remains because of the two-terminal measurement technique used. The observed temperature dependence of the $c$-axis resistance clearly reflects the characteristic behavior of a slightly underdoped Bi2212 single crystal, typical of Bi2212 THz-emitters.[4,7–12]

For the detection of the EM waves from the SAM, we used a Si-composite bolometer (Infrared Laboratories) as a detector. The generated EM waves from the SAM device are modulated by an optical chopper with the frequency of ~70 Hz. These modulated EM waves were detected by the Si-bolometer, and the output signal from the bolometer is measured using a lock-in amplifier with a reference signal from the optical chopper. Further details of our experimental setup for the detection of EM waves from mesa devices were reported previously.[7–9,11,12]

We observed the EM waves from this sample in bath temperatures T$_b$ ranging from 35 K to 60 K. The strongest EM radiation was observed at 55 K. Here, we primarily describe
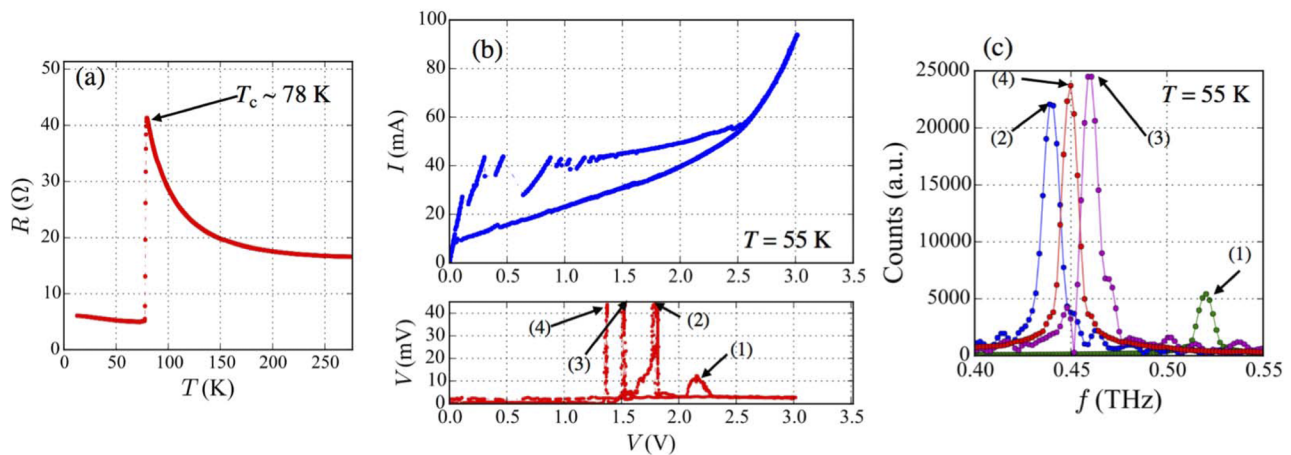
**FIG. 5**. (a) Temperature dependence of the *c*-axis resistance of the SAM. (b) IVCs and the applied bias voltage dependence of the bolometer output voltages at 55 K. (c) FT-IR spectrum obtained at the bias voltages points denoted (1)~(4) in (b).

the radiation characteristics of this sample observed at 55 K. The current-voltage characteristics (IVCs) of this sample at 55 K are shown in Fig. 5(b). The IVCs show a hysteresis loop during sweeps of the bias current/voltage up and down. It is well known that the hysteresis loop of IVCs strongly depends on $T_b$, as the size of the hysteresis loop shrinks with increasing $T_b$. The tendency of the temperature dependence of IVCs of this sample is a common behavior of previous samples fabricated using dry-etching methods.[7–9,11,12]

As displayed in Fig. 5(b), the radiation of EM waves is observed clearly on the return branch of the IVCs for which the dc voltage V is in the range 1.4~2.2 V. We also measured the V dependence of the radiation frequencies by using a Fourier transform infrared (FT-IR) spectrometer (FAIRS-1, JASCO). Note that because of the experimental conditions limiting the simultaneous measurements of the radiation power and frequency, the maximum peak displayed in Fig. 5(b) just indicates the tendency of the radiation output power intensity.

The observed radiation spectrum at the bias points denoted by (1) to (4) in the lower panel of Fig. 5(b) are shown in Fig. 5(c). At the strong radiation points denoted by (2), (3), and (4) on the IVCs, the radiation frequencies of about 0.45 THz were observed. It is noted that in the re-trapping IVC region, the number of working Josephson junctions can vary. This means that the effective voltage to the junctions may be varied step by step in the re-trapping region by decreasing V. This effect is included in the V dependence of the radiation frequency characteristics shown in Fig. 5(c).

According to previous studies of EM cavity modes in rectangular Bi2212 mesa structures, the resonance frequency, $f_c$, of the transverse magnetic mode TM(1,0) can be expressed as $f_c = c_0/(2n_r w)$, where $c_0$ is the speed of light in vacuum, $w$ is the width of the mesa structure, and $n_r \sim 4.2$ is the refractive index of Bi2212 single crystals as deduced from many previous experiments on samples at least 1$\mu$m in thickness.[4,7,8] The resonance frequency of the TM(1,0) mode of this sample can be estimated to be 0.45 ~0.53 from the width range of 71 ~83 $\mu$m mesa structure. Therefore, the radiation peaks shown in Fig. 5(c) can be naturally assigned to the TM(1,0) mode.

According to the experimental results of the $T_b$ dependence of the radiation frequencies $f$, the observed $f$ values from this sample decrease with increasing $T_b$, as observed commonly in previous studies of Bi2212-THz emitters fabricated using dry-etching techniques. This behavior is attributed to the shrinkage of the hysteresis loop of IVCs with increasing $T_b$. The applied V per junction decreases with increasing $T_b$. From this wet-etched SAM, we observed that $f$ varies from 0.41 to 0.54 THz by adjusting $T_b$ and V. The device characteristics so far obtained from this wet-etched sample show no difference from the mesas fabricated by using dry-etching methods. Therefore, the wet-etching method detailed here can effectively replace dry-etching methods of fabrication of the Bi2212-THz emitters without any significant differences in the emission properties.

## V. SUMMARY

We studied the effects of wet-etched Bi2212 single crystals using several different etching solutions. The results clearly showed that either some of the dilute concentrations of HCl or certain mixtures of diluted HCl and $HNO_3$ can be used as an effective etchant of Bi2212 single crystals. Although in many cases, the acid etchants penetrate underneath the photoresist on top of the sample, this "undercutting" of the sample can be significantly reduced by using a mixed water solution of dilute HCl and dilute $HNO_3$. Therefore, the particular etchant solution should be selected depending on the desired size and thickness of the mesa structures. In this study, we simultaneously fabricated seven stand-alone mesa structures by using a

mixed solution of dilute HCl and $HNO_3$. The fabricated mesa devices generated THz EM waves clearly and the observed radiation characteristics were very similar to that commonly observed from previous studies of stand-alone mesas fabricated using dry-etching methods. This result indicates clearly that the wet-etching method can be applied to the fabrication of efficient Bi2212-THz emitters. In addition, this method is useful to make any two-dimensional shape of mesa structures in a very short time, allowing for their inexpensive mass production.

## ACKNOWLEDGMENTS

## REFERENCES

[1] R. Kleiner, F. Steinmeyer, G. Kunkel, and P. Müller, Phys. Rev. Lett. **68**, 2394 (1992).

[2] R. Kleiner and P. Müller, Phys. Rev. B **49**, 1327 (1994).

[3] A. A. Yurgens, Superconductor Science and Technology **13**, R85 (2000).

[4] L. Ozyuzer, A. E. Koshelev, C. Kurter, N. Gopalsami, Q. Li, M. Tachiki, K. Kadowaki, T. Yamamoto, H. Minami, H. Yamaguchi, T. Tachiki, K. E. Gray, W.-K. Kwok, and U. Welp, Science **318**, 1291 (2007).

[5] B. Josephson, Physics Letters **1**, 251 (1962).

[6] H. Minami, I. Kakeya, H. Yamaguchi, T. Yamamoto, and K. Kadowaki, Applied Physics Letters **95**, 232511 (2009).

[7] K. Kadowaki, M. Tsujimoto, K. Yamaki, T. Yamamoto, T. Kashiwagi, H. Minami, M. Tachiki, and R. A. Klemm, Journal of the Physical Society of Japan **79**, 023703 (2010).

[8] M. Tsujimoto, K. Yamaki, K. Deguchi, T. Yamamoto, T. Kashiwagi, H. Minami, M. Tachiki, K. Kadowaki, and R. A. Klemm, Phys. Rev. Lett. **105**, 037005 (2010).

[9] T. Kitamura, T. Kashiwagi, T. Yamamoto, M. Tsujimoto, C. Watanabe, K. Ishida, S. Sekimoto, K. Asanuma, T. Yasui, K. Nakade, Y. Shibano, Y. Saiwai, H. Minami, R. A. Klemm, and K. Kadowaki, Applied Physics Letters **105**, 202603 (2014).

[10] M. Ji, J. Yuan, B. Gross, F. Rudau, D. Y. An, M. Y. Li, X. J. Zhou, Y. Huang, H. C. Sun, Q. Zhu, J. Li, N. Kinev, T. Hatano, V. P. Koshelets, D. Koelle, R. Kleiner, W. W. Xu, B. B. Jin, H. B. Wang, and P. H. Wu, Applied Physics Letters **105**, 122602 (2014).

[11] T. Kashiwagi, K. Sakamoto, H. Kubo, Y. Shibano, T. Enomoto, T. Kitamura, K. Asanuma, T. Yasui, C. Watanabe, K. Nakade, Y. Saiwai, T. Katsuragawa, M. Tsujimoto, R. Yoshizaki, T. Yamamoto, H. Minami, R. A. Klemm, and K. Kadowaki, Applied Physics Letters **107**, 082601 (2015).

[12] T. Kashiwagi, T. Yamamoto, T. Kitamura, K. Asanuma, C. Watanabe, K. Nakade, T. Yasui, Y. Saiwai, Y. Shibano, H. Kubo, K. Sakamoto, T. Katsuragawa, M. Tsujimoto, K. Delfanazari, R. Yoshizaki, H. Minami, R. A. Klemm, and K. Kadowaki, Applied Physics Letters **106**, 092601 (2015).

[13] D. Y. An, J. Yuan, N. Kinev, M. Y. Li, Y. Huang, M. Ji, H. Zhang, Z. L. Sun, L. Kang, B. B. Jin, J. Chen, J. Li, B. Gross, A. Ishii, K. Hirata, T. Hatano, V. P. Koshelets, D. Koelle, R. Kleiner, H. B. Wang, W. W. Xu, and P. H. Wu, Applied Physics Letters **102**, 092601 (2013).

[14] S. Sekimoto, C. Watanabe, H. Minami, T. Yamamoto, T. Kashiwagi, R. A. Klemm, and K. Kadowaki, Applied Physics Letters **103**, 182601 (2013).

[15] T. M. Benseman, K. E. Gray, A. E. Koshelev, W.-K. Kwok, U. Welp, H. Minami, K. Kadowaki, and T. Yamamoto, Applied Physics Letters **103**, 022602 (2013).

[16] E. A. Borodianskyi and V. M. Krasnov, Nature Communications **8**, 1742 (2017).

[17] Q. Lu, D. Wu, S. Sengupta, S. Slivken, and M. Razeghi, Scientific Reports **6**, 23595 EP (2016).

[18] T. Maekawa, H. Kanaya, S. Suzuki, and M. Asada, Applied Physics Express **9**, 024101 (2016).

[19] M. Tonouchi, Nature Photonics **1**, 97 EP (2007).

[20] U. Welp, K. Kadowaki, and R. Kleiner, Nature Photonics **7**, 702 EP (2013).

[21] I. Kakeya and H. Wang, Superconductor Science and Technology **29**, 073001 (2016).

[22] T. Kashiwagi, H. Kubo, K. Sakamoto, T. Yuasa, Y. Tanabe, C. Watanabe, T. Tanaka, Y. Komori, R. Ota, G. Kuwano, K. Nakamura, T. Katsuragawa, M. Tsujimoto, T. Yamamoto, R. Yoshizaki, H. Minami, K. Kadowaki, and R. A. Klemm, Superconductor Science and Technology **30**, 074008 (2017).

[23] T. Kato, H. Ishida, H. Suematsu, K. Yasui, and K. Hamasaki, Cryogenics **52**, 398 (2012).

[24] T. Nishikata, T. Kato, Y. Kotaki, H. Suematsu, A. Kawakami, and K. Yasui, Japanese Journal of Applied Physics **53**, 04EJ02 (2014).

[25] E. A. Vopilkin, A. V. Chiginev, L. S. Revin, A. N. Tropanova, I. Y. Shuleshova, A. I. Okhapkin, A. D. Shovkun, A. B. Kulakov, and A. L. Pankratov, Superconductor Science and Technology **28**, 045006 (2015).

[26] R. A. Klemm and K. Kadowaki, Journal of Superconductivity and Novel Magnetism **23**, 613 (2010).

[27] R. A. Klemm and K. Kadowaki, Journal of Physics: Condensed Matter **22**, 375701 (2010).

[28] T. Mochiku, K. Hirata, and K. Kadowaki, Physica C: Superconductivity **282-287**, 475 (1997), proceedings of the International Conference on Materials and Mechanisms of Superconductivity High Temperature Superconductors V Part II.